Version of Record: https://www.sciencedirect.com/science/article/pii/S0169433220331056
Manuscript_0c5b2bdf102e63d166379c68a070780d

Controlling N and C-atom densities in N_2/H_2 and N_2/CH_4 microwave afterglows for selective TiO_2 surface nitriding

Andre Ricard[a*], *Yunfei Wang*[b†], *Yoon Sang Lee*[b,c], *Jean-Philippe Sarrette*[a], *Ansoon Kim*[c] *and Yu Kwon Kim*[b*]

[a]LAPLACE, Université de Toulouse, CNRS, INPT, UPS, 118 route de Narbonne, 31062 Toulouse, France
[b]Department of Energy Systems Research, Ajou University, Suwon 16499, Korea
[c]Korea Research Institute of Standards and Science (KRISS), Gajeongro 267, Yuseong-gu, Daejeon 34113, South Korea

[*]Corresponding authors: yukwonkim@ajou.ac.kr (Y. K. Kim), ricard@laplace.univ-tlse.fr (A. Ricard)

[†]Present address: School of Chemistry & Materials Engineering, Xinxiang University, Xinxiang 450003, China

Abstract

Radiative states of N_2/<5% H_2 and N_2/<5$^0/_{00}$ CH_4 HF(microwave) flowing afterglows of microwave plasmas at reduced gas pressures (4-20 Torr) have been analyzed by emission spectroscopy. The N_2 1st pos (580 nm), 2nd pos (316 nm), N_2^+ 1st neg (391.4 nm), NH (336 nm) and CN (386 nm) bands in the pink (early) and the late afterglows were measured and the NO titration was used to determine the concentrations of N-atoms, O-atoms in impurity, N_2(X,v>13) and N_2(A) metastable molecules, N_2^+ ions. Introduction of small percentages of H_2 (or CH_4) into N_2 lead to a size reduction of the early afterglow region which was followed by a late afterglow zone where the N + N recombination is the dominant process. In addition, it also gave an effect of reducing the densities of N atoms (as well as the N_2 excited states) in the afterglow regions. At the same time, it introduced other active species such as H (or C) atoms, of which the densities strongly vary depending on the percentage of H_2 (or CH_4) in the mixture. Such changes in the densities of active species such as N and C atoms in the afterglow region had a strong influence on the incorporation reaction rates of N atoms into the surface of TiO_2 films introduced into the afterglow region. These results deliver an important meaning in devising process conditions especially for selective nitrogen or carbon doping into a skin-depth layers of oxide materials, which is desired in the case of preparing functional films for photoelectric and photocatalytic applications.

Key words microwave afterglows; emission spectroscopy; N and C-atoms densities; TiO_2 ; surface nitriding

© 2020 published by Elsevier. This manuscript is made available under the CC BY NC user license
https://creativecommons.org/licenses/by-nc/4.0/

1. Introduction

N_2 and N_2/H_2 flowing microwave (2.45 GHz) afterglows have been intensively studied in the past by emission spectroscopy [1-3], which gives information on the type and the densities of excited states of molecules and ions in the afterglows. By studying the emission spectra of the early and late afterglows, the detailed reaction kinetics of the N atoms, the $N_2(X,v)$ vibrationally excited ground state, the N_2(A and a′) metastable molecules and the N_2^+ ions have been studied intensively in pure N_2 and are now well-understood as described in the previous literatures [4-6].

For the determination of the N-atom density in the afterglows, a simple method such as NO titration has been successfully employed as described elsewhere [1, 2]. Then, the concentrations of other active species such as N_2(A), $N_2(X,v>13)$ metastable molecules, N_2^+ ions and O-atoms (possibly from microleaks or impurities in the gas tank) are determined from the well-established method of band-ratio intensities [1, 2]. This method has been successfully employed in determining the densities of various active species not only in pure N_2 afterglows, but also in the mixtures of N_2-H_2 [7, 8].

Such an information on the densities of active species in the afterglows may be used in evaluating and understanding nitridation processes, especially when a mild treatment condition in the post-discharge (afterglow) region is desired as in the case of surface-selective modification of skin-depth layer of oxide materials such as TiO_2 for controlling catalytic and photocatalytic activities [9, 10]. Interesting results have been observed recently from the studies on nitridation of TiO_2 in the N_2 and N_2-H_2 afterglows [7, 8, 11]. Controlling the type of active species such as oxygen impurities and N_2^+ ions in the N_2 afterglows was found to be responsible for the introduction of different types of surface N bonding states on TiO_2 [8]. High concentration of N atoms over that of N_2^+ ions as in the late afterglows was found to be effective in enhancing surface nitridation performances [11]. The presence of H atoms as in the N_2/H_2 afterglows of microwave discharges may reduce the surface nitridation performance at room temperature due to the surface passivation by H atoms [11], but leads to enhanced N incorporation rate at elevated temperatures since the reaction of H atoms may deplete the surface oxygen atoms for further incorporation of N atoms followed by subsequent diffusion into the subsurface [7]. In this way, the addition of H_2 into N_2 enhances the N incorporation rate into the subsurface, thus the nitriding of TiO_2 can be performed at lower substrate temperatures.

The interest on the N_2/CH_4 plasma and afterglows has been also established for various applications such as nitrocarburizing iron surfaces [12], the formation of nanostructured carbon films [13] and the C,N-co-doping of TiO_2 for enhanced photocatalyst applications [14]. The condition with the maximum densities of N and C atoms in the afterglows can be chosen by monitoring the emission spectra. Iron metals exposed to the afterglows at an elevated temperature were found to have a surface nitride layer with a few percent of C incorporated. A similar treatment of TiO_2 in the N_2/CH_4 afterglows may be also useful in

preparing oxynitride layers of a well-defined thickness on TiO_2 possibly with a few percent carbon incorporated for enhanced photocatalytic performances [15-17].

In the present study, active species produced in N_2/<5% H_2 and N_2/<5$^0/_{00}$ CH_4 afterglows are optimized by varying the discharge conditions and their densities are thoroughly examined for use in surface nitriding of TiO_2. Absolute concentrations of N-atoms, O-atoms in impurity, $N_2(X,v>13)$ and $N_2(A)$ metastable molecules and N_2^+ ions are monitored in N_2/<5% H_2 HF afterglows, using band intensity ratios [1, 2, 8, 18]. The method allows the determination of absolute C-atoms densities in N_2/<5$^0/_{00}$ CH_4 afterglows. The ratios of H_2 (or CH_4) in the mixture examined in this study are those that can generate high concentrations of active species in the afterglow region as determined in the previous studies [8, 12, 18]. The detailed experimental conditions of generating the HF afterglows are also presented. The comparison shows again that the small amount of H_2 (or CH_4) induces a large perturbation in the densities of active species in the afterglows. A rapid evaluation of nitriding performances of TiO_2 also shows an interesting variation in the nitriding rate depending on the type of active species in the afterglows.

2. Experimental setup

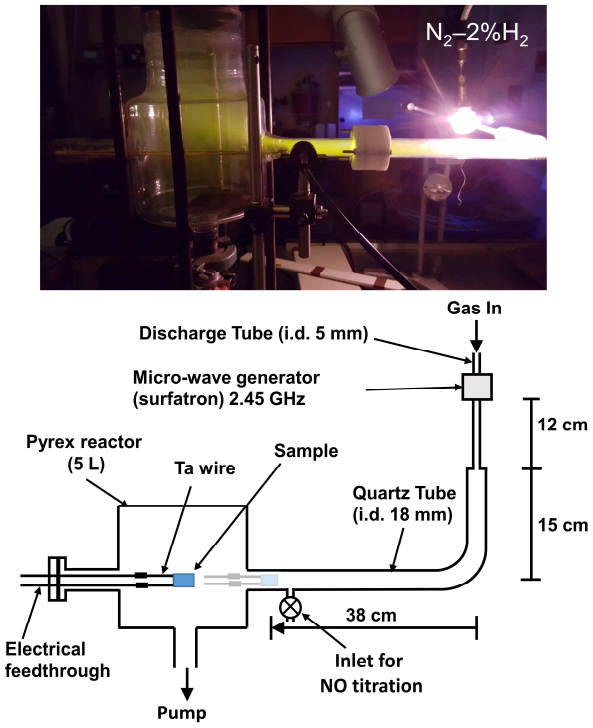


Fig. 1. Photo and scheme of the microwave flowing afterglow experimental setup. The sample can be heated in the 5 litre reactor or in the 18 mm i.d. tube for surface treatment in the afterglow region.

The experimental set-up of the microwave afterglow is reproduced in Fig. 1. The N_2 and other gas (H_2 or CH_4) flows are introduced into the discharge quartz tube with the internal diameter (i.d.) of 5 mm, which goes through a surfatron cavity.

The microwave plasma is generated by the surfatron when a microwave (2.45 GHz) power of 100 W is applied. The discharge tube extends further after the surfatron by about 12 cm and is connected to a 50 cm-long bent quartz tube of 18 mm i.d., which is connected to a 5 liters Pyrex chamber.

A sample can be introduced into the chamber and can be heated up to 600 K (see Fig.1) inside the reactor or in the 18 mm i.d. tube, at a distance z = 38 cm from the bent tube inlet. The position at z = 38 cm corresponds to an afterglow time of 10^{-1}s and is the sample position used in this study for the surface treatment of TiO_2 films.

Optical emission spectroscopy is performed by means of an optical fiber connected to an Acton Spectra Pro 2500i spectrometer (grating 600 gr/mm) equipped with a Pixis 256E CCD detector (front illuminated 1024 x 256 pixels). The plasma and afterglows spectra are characterized by the emission of the N_2 1^{st} pos system and CN-red bands in the red part of the spectrum between 500 and 1100 nm and by the emissions of the N_2 2^{nd} pos, N_2^+ 1^{st} neg ,NO_β (320 nm), NH (336 nm) and CN (388 and 385 nm) in the UV-blue part between 300 and 400 nm.

The discharge in the surfatron is followed by afterglows which appear usually in the quartz tube at the downstream. A pink afterglow is observed in the bent part of the 18 mm i.d. tube at z = 15 cm (27 cm from the surfatron) with a N_2 flow rate of 0.5 slpm, a pressure p = 5 Torr and a microwave power of 100 W. After the pink afterglow, the late afterglow follows and appears in the quartz tube after the bent region. NO titration can be performed for absolute N-atom density calibration in the late afterglow region by introducing an Ar-1.5%NO flow (see Fig.1).

3. N_2 pink and late afterglows

A pink afterglow was detected in the shoulder of the 18 mm i.d. tube at z = 15 cm (5 10^{-2}s). Table 1 summarizes absolute active species densities obtained from band intensity ratios [1, 2, 8, 18], shown versus the distance from z = 13 cm (5 10^{-2}s) to 38 cm (10^{-1}s) at 8 Torr, 0.5 slpm and 100 W.

In this Table, the a_{N+N} factor indicates the proportion of the N_2 1^{st} pos intensity (I_{580}) emitted at 580 nm ($N_2(B,v'=11) \rightarrow N_2(A,v''=7)$ vibrational transition) due to the three body recombination $N + N + N_2 \rightarrow N_2(B,v'=11) + N_2$: $a_{N+N} = 0$ for a pure pink afterglow and $a_{N+N} = 1$ for a pure late afterglow.

It is found that the densities of the N-atoms and of the $N_2(X,v>13)$ metastable molecules (sum of the $N_2(X)$ vibrational levels higher than v=13) remain at (1-2) 10^{15}cm^{-3} for N–atoms

and (0.6-1.0) $10^{14}cm^{-3}$ for $N_2(X,v>13)$ molecules from z = 13 cm to 38 cm. However, the concentrations of the $N_2(A)$ metastable molecules and the N_2^+ ions decrease as the gas flows from the pink (z = 15 cm) to the late afterglow region (z = 38 cm). The O-atom density slowly increases from 3 to 9 $10^{13}cm^{-3}$, corresponding to a $[O]/[N_2]$ ratio varying between 0.1 and 0.3 10^{-3}.

In the 5 liters reactor, a maximum of the N-atom density is obtained at 5 Torr, 0.5 slm and 100 W, where it is measured [N] = 5 $10^{14}cm^{-3}$ and [O] = 3.5 $10^{13}cm^{-3}$, by assuming an homogenous N-atom spatial distribution, which is about half the values measured in the 18 mm i.d. tube at z = 38 cm (10^{-1}s).

z (cm)	13	15	17	19	38
a_{N+N}	0.2	0.3	0.45	0.6-0.7	1.0
[N] ($10^{15}cm^{-3}$)	0.9	1.0	1.2	1.4-1.8	2.0
[O] ($10^{13}cm^{-3}$)	3.3	4.0	4.0	4.0-7.0	9.0
$[N_2(A)]$ ($10^{11}cm^{-3}$)	2.3-4.0	2.4	1.7	1.3-1.6	-
$[N_2(X,v>13)]$ ($10^{14}cm^{-3}$)	0.6-1.0	0.7	0.7	0.6-0.7	-
$[N_2^+]$ ($10^{10}cm^{-3}$)	20.0	2.0	0.5	0.4-0.5	-

Table 1. N_2 active species densities in the afterglow at 8 Torr, 0.5 slpm, 100 W.

4. N_2/<5%H_2 plasma and early afterglow

For comparison with that of pure N_2, the discharge condition has been chosen to be N_2/2%H_2, 5 Torr, 0.5 slpm, 100 W. Active species densities were measured in the afterglow at 3 different positions along the 18 mm i.d. tube at z = 5, 13 and 38 cm and inside the 5 litres reactor.

The results are reported in Table 2. The $N_2(A)$ density is below the measurement limit (< $10^{11}cm^{-3}$ in the 5 litres reactor. As for the $N_2(X,v>13)$ metastable and N_2^+ ion concentrations ,

they cannot be obtained at z = 38 cm and in the 5 litres reactor as the a_{N+N} factor was found to be equal to 1 (pure late afterglow).

The role of 2% H_2 added to N_2 here can be clearly identified from the changes of the N-atom density in the afterglow region. It decreased by a factor of 3-4 when going from z = 38 cm to the 5 litre reactor that is more than in pure N_2 where it was observed a decrease by a factor of about 2. Thus, the decrease in the N atom density along the gas flow in the afterglow region is even more in the N_2/2%H_2 case than in the pure N_2 case.

z (cm)	5	13	38	reactor
a_{N+N}	0.40	0.50	1.00	1.00
[N] ($10^{14}cm^{-3}$)	8.0	9.0	11.0	3.0
[O] ($10^{13}cm^{-3}$)	2.0	1.4	0.4	0.2
[N_2(A)] ($10^{11}cm^{-3}$)	5.0	2.0	0.7	-
[N_2(X,v>13)] ($10^{13}cm^{-3}$)	1.3	3.0	-	-
[N_2^+] ($10^{10}cm^{-3}$)	4.5	0.4	-	-

Table 2. N_2/2%H_2 active species densities determined at 5 Torr, 0.5 slpm, 100 W for different z positions.

The O-atom density is found to strongly decrease in the reactor by adding 2%H_2 to N_2, from 3.5 10^{13} to 0.2 10^{13} cm^{-3}. At z = 13 cm, the density of the N_2^+ ions is reduced by one order of magnitude, compared with the one determined in the N_2 pink afterglow. Such a decrease is the result of the efficient charge transfer reaction : $N_2^+ + H_2 \rightarrow N_2H^+ + H$ with a rate constant of 2 $10^{-9}cm^3s^{-1}$ [3, 19].

Afterall, the introduction of 2% H_2 into the N_2 flow has an effect of reducing the densities of N atoms (down to a half) and other excited N_2 and N_2^+ states (down to a detection limit). The presence of NH and H species (as detected in the emission spectra [7]) provides a reducing environment which suppresses the density of O atoms (from O_2 impurity) as well. Such a change in the type and the densities of active species in the afterglow region has shown to have a huge impact on the overall nitridation performance of TiO_2 films exposed to the afterglow [7].

5. N_2/<5⁰/₀₀CH_4 HF afterglow

The $N_2/<5\%_{00}CH_4$ HF afterglows are specifically studied with application in post-treatments of the oxide films such as TiO_2 in mind.

In the plasma, the CH_4 molecules are in part dissociated by electron collisions in C and H atoms. In addition in the afterglow, the C-atoms are produced by the following reactions :

$$N + CH_x \rightarrow CN + xH \qquad (a)$$

with $k_a = (1\text{-}2)\ 10^{-10} cm^3 s^{-1}$ for x = 3 [20], followed by the efficient reaction:

$$N + CN \rightarrow C + N_2 \quad \text{with } k_b = 10^{-10}\ cm^3 s^{-1} \qquad (b)$$

As indicated in [12], the C-atom density can be deduced in the late afterglow region from the CN(B,7-X,7) band intensity at 385 nm shown in Fig. S1, as the CN(B,7) level is essentially produced by the following reaction :

$$C + N + N_2 \rightarrow CN(B,7) + N_2 \qquad (c)$$

with $k_c = 9\ 10^{-33}\ cm^6 s^{-1}$ [20].

The I_{385} intensity is given from reaction (c) by :

$$I_{385} = k_1\,[C]\,[N] \qquad (1)$$

$$\text{with } k_1 = \frac{c(385)}{385} A^{(B,7)}_{(X,7)} \frac{kc[N_2]}{(\nu^R_{CN(B,7)} + [N_2]k^Q_{CN(B,7)})}$$

where c(385) is the spectral response of the spectrometer in arbitrary units for the wavelength λ = 385 nm, $A^{(B,7)}_{(X,7)}$ is the probability of the CN(B,7-X,7) transition, k_c is the rate coefficient for reaction (c), $\nu^R_{CN(B,7)}$ and $k^Q_{CN(B,7)}$ are the radiative frequency of the CN(B,7) state and its quenching rate coefficient by the N_2 molecule, respectively [20].

The absolute N-atom density in eq. (1) is determined by NO titration. The I_{580} intensity reduced by a_{N+N} (see part 3) is as follows [1, 2]:

$$a_{N+N} \cdot I_{580} = k_2[N]^2 \qquad (2)$$

$$\text{with } k_2 = \frac{c(580)}{580} A^{(B,11)}_{(A,7)} \frac{k_d[N_2]}{(\nu^R_{N_2(B,11)} + [N_2]k^Q_{N_2(B,11)})}$$

where k_d is the rate coefficient of the 3-body $N + N + N_2 \rightarrow N_2(B,11) + N_2$ recombination reaction [1, 2].

The C-atom density is then deduced from the N-atom density by the following intensity ratio :

$$a_{N+N} \cdot \frac{I_{580}}{I_{385}} = \frac{k_2}{k_1} \frac{[N]}{[C]} \qquad (3)$$

To investigate into the active species densities of the N_2/CH_4 HF afterglows, the following parameters were chosen: $N_2/x\%CH_4$ with x varying from 0.04 to 0.3, P = 9-13 Torr, Q = 0.5 slpm and P_{HF} = 100 W.

Spectra of the $N_2/0.04\%CH_4$ afterglow recorded in the 5 litres reactor at 9 Torr, 0.5 slpm and 100 W are reproduced in the 300-400 nm (Fig. S1a) and 520-620nm (Fig. S1b) range.

The CN(B,7-X,7) band at 385 nm (Fig. S1a) is produced by reaction (c). It superimposes with the CN(B,0-X,0) and CN(B,1-X,1) bands at 388 and 387 nm, respectively.

The origin of the I_{385} intensity was measured at the middle of the CN(1-1) rotational band extension. The CN(0-0) band emission could be the result of the following reaction :

$$N_2(X,v>12) + CN \rightarrow CN(B,0) + N_2 \qquad (d)$$

with the rate coefficient $k_b = 1.7\ 10^{-11}\ cm^3s^{-1}$ [21].

Other reactions are found in previous works to produce the CN(B,0) excited state such as: $N + CH_x \rightarrow CN(B,0) + xH$ and $CNH_2^+ + e \rightarrow CN(B,0) + H_2/2H$ [22].

The N_2(B,11-A,7) band at 580 nm (Fig. S1b) is clearly identified, mixed with the CN(A,v') → CN(X,v") red bands at 575 nm (5-1), 588 nm (6-2) and 601 nm (7-3). To avoid the perturbation caused by the CN emission at 588 nm, the a_{N+N} factor in eqs. (2) and (3) was obtained using the I_{580}/I_{585} band intensity ratio from N_2(B,11) to N_2(B,10) instead of the I_{580}/I_{590} ratio from N_2(B,11) to N_2(B,9) as indicated in [1, 2].

Under the given condition, the afterglow inside the 5 litre reactor is observed to be clearly inhomogeneous. It has been observed that the N and C atom densities are, respectively, 2 and 3 times lower at the reactor bottom than in the center.

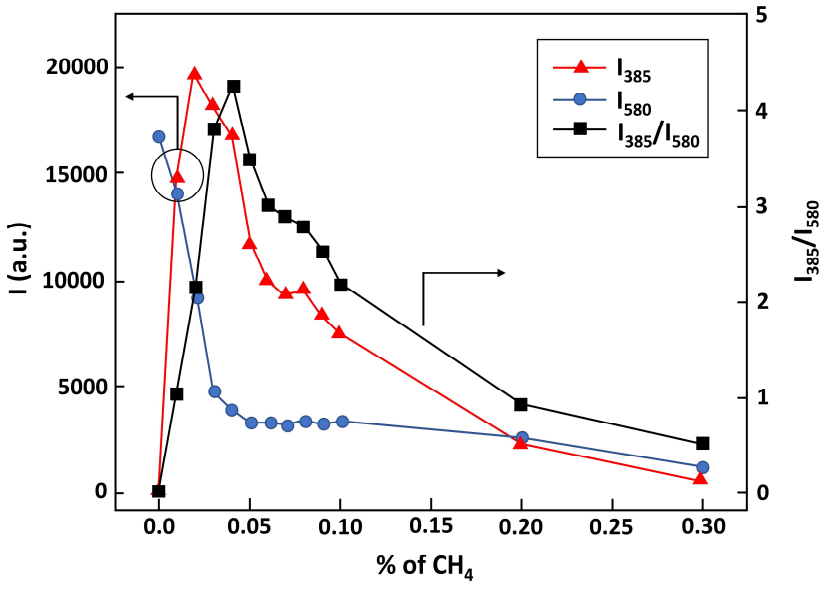


Fig. 2 Variations of I_{385} , I_{580} intensities and of the I_{385}/I_{580} intensity ratio in the N_2/xCH_4 mixtures with x<0.3% for p = 13 Torr, z = 38 cm, Q = 0.5 slpm and P_{HF} = 100 W.

At z = 38 cm, the HF afterglow is a homogenous late afterglow (a_{N+N} =1). The densities of C and N atoms at the late afterglow region are deduced from the analysis of emission lines at 385 and 580 nm. In Fig. 2, the emission intensities of I_{385} and I_{580} as well as the I_{385}/I_{580} intensity ratio are shown against the $\%CH_4$ in the N_2-CH_4 mixture. The I_{580} intensity which is proportional to $[N]^2$ (eq. 2) sharply decreases with increasing $\%CH_4$ as a result of reaction (a). The I_{385} intensity which follows [C][N] (eq. 1) is related to C production by CN collisions though reaction (b). It increases up to about 0.03 $\%CH_4$ then decreases. Considering the kinetics behind the I_{385} and I_{580} intensities discussed above (eqs. 1 and 2), the I_{385}/I_{580} ratio is proportional to the [C]/[N] ratio (eq. 3) and is found to show a maximum at about 0.05 % CH_4 (see Fig. 2).

With $k_2/k_1 = 1.2\ 10^{-2}$ in eq. (3), the [C]/[N] density ratio is directly deduced from the I_{385}/I_{580} intensity ratio in Fig. 2. The [C]/[N] value at the maximum I_{385}/I_{580} is calculated to be 5 %. As N atom density quickly decreases with the $\%CH_4$, the increase of C atoms at $<0.05\%CH_4$ appears to be the result of a quick CN production in part by reaction (a). At higher CH_4 percentages (>0.05%), the N-atom density being stabilized, the decrease of C atom density is the result of rapid exothermic reactions between C and CH_x (e.g., $C + CH_4 \rightarrow H + C_2H_3$) [23].

The discharge condition can be adjusted to maximize the N and C atom densities in the afterglow since high densities of N and C atoms in the afterglow are expected to be advantageous for surface nitriding of TiO_2 with co-doped C.

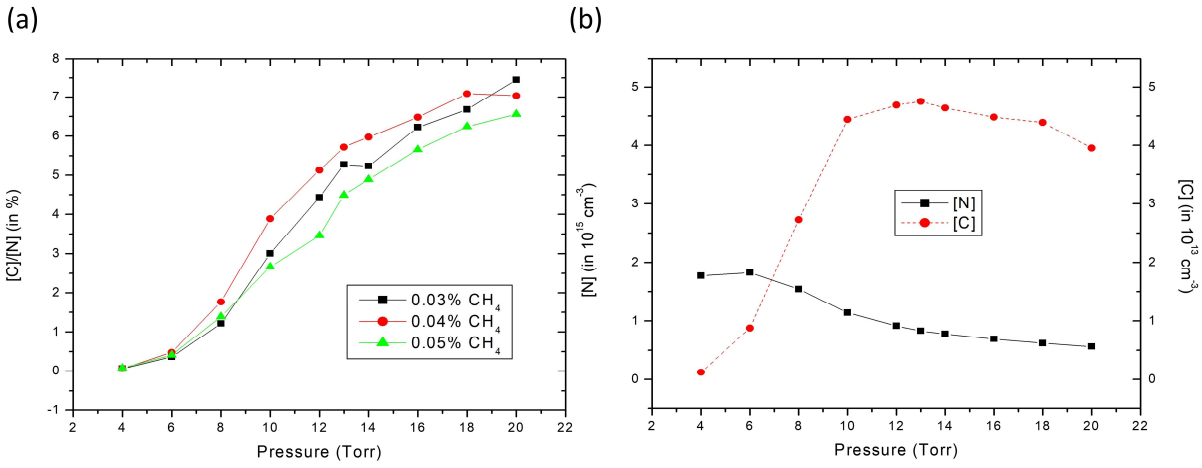


Fig. 3. Variation of the [C]/[N] ratio for different $N_2/x\%CH_4$ mixtures (a) and variation of [C] and [N] densities for the $N_2/0.04\%CH_4$ mixture (b) plotted against pressure measured at the conditions of z = 38 cm, Q = 0.5 slpm and P_{HF} = 100 W.

Fig. 3 shows pressure-dependent changes in the [C]/[N] ratio (a) as well as in the absolute densities of C and N atoms (b) at the late afterglow (z = 38 cm). Fig. 3a indicates that the [C]/[N] ratio increases monotonously as the gas pressure increases from 6 and 14 Torr. At higher pressures, the ratio approaches to a saturation value. Similar pressure-dependent trend is observed when the CH_4 ratio is varied between 0.03 to 0.05 % in the N_2/(0.03-0.05)%CH_4 mixtures, but is maximized at the CH_4 ratio of 0.04 % (in the N_2/0.04%CH_4 mixture). Nevertheless, since the C–atom density reaches a maximum between 10 and 16 Torr in this mixture (Fig. 3b), 13 Torr was chosen for comparison. At this pressure, both the [C]/[N] ratio and the [C] absolute concentration are determined to be at 5 % and about 5 10^{13} cm^{-3}, respectively, at the position z = 38 cm.

In Table 3, it is compared the N and C-atoms densities at z = 38 cm and inside the 5 litres reactor for the N_2/4 $10^{-4}CH_4$ gas mixture. It is observed as for the N_2-2%H_2 (Table 2) a density decrease in the reactor by a factor 3-4 .

z (cm)	38	reactor
a_{N+N}	0.6-1.0*	1.0
[N] ($10^{15}cm^{-3}$)	1- 1*	0.35
[C] ($10^{13}cm^{-3}$)	3- 5*	0.7

Table 3. N_2/4 $10^{-4}CH_4$ active species densities determined at 9 Torr, 0.5 slpm, 100 W for z = 38 cm and inside the reactor.* results at 13 Torr

Active species production in the afterglows was compared in N_2-H_2 mixtures and in Ar-N_2-H_2 mixtures with dominant Ar gas in earlier studies [1, 2]. In the present paper, the production of N and C atoms was similarly analyzed as is done in Ar-N_2-CH_4 gas mixtures for comparison with those in the N_2-CH_4 case. To compare with the results presented in Fig.3b for N_2/*x*%CH_4 afterglows, it is chosen the Ar/4%N_2/0.04%CH_4 gas mixture. At 13 Torr, 0.5 slpm, 100 W, z = 38 cm, it is measured a_{N+N} = 0.4, [N] = 6 10^{14} cm^{-3} and [C] = 4 10^{12} cm^{-3}. By comparison, the results were reported for the same conditions (*) in Table 3. When the Ar-N_2-H_2 gas mixture is used, the late afterglow fraction (a_{N+N}) at z = 38 cm decreases from 100% to 60%. The [N]/[N_2] ratio increased from 0.2% to 3.5%, corresponding to about 20 fold increase while the [C]/[N_2] ratio only increased from a factor 2, varying from 1 to 2 10^{-4}. The introduction of Ar as a dominant gas was thus more beneficial to the [N]/[N_2] ratio than to the [C]/[N_2] ratio. However, the absolute densities of N and C-atoms are lower for the Ar-N_2-H_2 gas mixture by a factor of about 2 and 10, respectively, than for the N_2-H_2 gas mixture.

Thus, it is concluded that high densities of N and C atoms in the afterglows for efficient nitriding of TiO_2 can be achieved more easily without Ar dilution in the N_2/CH_4 case.

6. TiO_2/Si substrate treatments

Finally, the TiO_2 films (anatase, about 100 nm) grown on Si substrates are exposed to three different microwave afterglows of N_2, $N_2/2\%H_2$ and $N_2/0.04\%CH_4$, respectively to understand the effect of the varying active species densities in the afterglow region on nitridation performances of the TiO_2 films. For the surface treatment, the sample was positioned at z = 38 cm in the quartz tube and the substrate was resistively heated up to 300 °C for 30 min (see Fig.1). Under the given discharge conditions (Q_{tot} = 0.5 slpm, P_{HF} = 100 W), the N and C atom densities are determined as follows:

N_2 only at 5 Torr : [N] = 5 10^{14}cm^{-3}, [O] = 5 10^{14}cm^{-3}

$N_2/2\%H_2$ at 5 Torr : [N] = 1 10^{15}cm^{-3}, [O] = 4 10^{12}cm^{-3}, [N_2(A)] = 7 10^{10}cm^{-3}

$N_2/0.04\%CH_4$ at 13 Torr : [N] = 1 10^{15}cm^{-3}, [C] = 5 10^{13}cm^{-3}, [O] = 4 10^{12}cm^{-3}, [N_2(A)] = 7 10^{10}cm^{-3}

The density of O-atoms in impurity was strongly decreasing by about two orders of magnitude when $2\%H_2$ was added to N_2.

After the exposure to the full late afterglows (a_{N+N}=1), the bonding states and the distribution of N species incorporated into the TiO_2 film were examined by taking X-ray photoelectron spectroscopy (XPS) spectra with successive removal of skin-depth surface layers by a stepwise sputtering with Ar_{2500}^+ ion beam (depth profile analysis). XPS measurements were performed in a PHI5000 Versa Probe II (Ulvac-PHI) system using a monochromatic Al Kα source. In this experimental setup, the X-ray beam diameter can be set to 200 μm and a dual charge neutralizer is used to minimize an undesirable charging effect. For the depth profile analysis, Ar gas cluster ion beam (Ar-GCIB, ULVAC-PHI) operating with Ar_{2500}^+ at 7 keV (sample current = 14 nA) was used to obtain a fairly uniform non-selective sputtering rate of about 0.1 – 0.3 nm/min. Furthermore, Zalar rotation of sample holder during Ar-GCIB sputtering was performed to minimize surface roughness and reduce cone formation.

Under the sputtering condition, the preferential sputtering effect of conventional Ar^+ ion sputtering is significantly suppressed and the chemical states and stoichiometry of Ti and O within the TiO_2 film are found to remain at mostly Ti^{4+} and O^{2-}. This provides an additional benefit in tracking down the chemical bonding states of N within the TiO_2 film during the sputter analysis. As a result of that, in the present study, the substitutional and interstitial N species are successfully resolved during the depth profile analysis.

All representative core level spectra of Ti 2p, N 1s, C 1s and O 1s core levels from the TiO_2 film treated in the N_2 afterglow (Fig. S2) show characteristic features of TiO_2 film. Ti $2p_{3/2}$ at 459 eV and O 1s at 530 eV represent Ti^{4+} and O^{2-} states of bulk TiO_2. N 1s features at 400 – 402 eV and 396 eV (Fig. S2) explain that interstitial (~ 400 eV) and substitutional (~ 396 eV) N species are incorporated into the film after the treatment in the afterglow [14, 24]. The C 1s feature at 284.8 eV comes from the ubiquitous hydrocarbon from the air. After the sputtering for a few minutes (< 1 nm), the dominant C feature disappears confirming that it originates from the airborne contaminant. The N 1s features are also reduced, but remain down to a few nm, suggesting that the subsurface incorporation of N into the bulk of TiO_2 has been achieved during the afterglow treatment. The sputtering also removes surface OH and chemisorbed H_2O species (532~ 533 eV) from O 1s spectra and leaves only the bulk oxide peak at 530 eV [11]. Sputtering does give a slight change in the Ti $2p_{3/2}$ feature toward lower binding energies due to a preferential sputtering of oxygen, but, this time, is quite suppressed due to the beneficial role of the Ar cluster ion beams, as discussed above. The commonly observed preferential sputtering effect of conventional Ar^+ ion sputtering has been significantly suppressed by using the optimized Ar cluster ion beam sputtering condition. Other than that, no significant changes in the Ti 2p and O 1s core level features are observed in the course of the Ar sputtering down to a few tens nm.

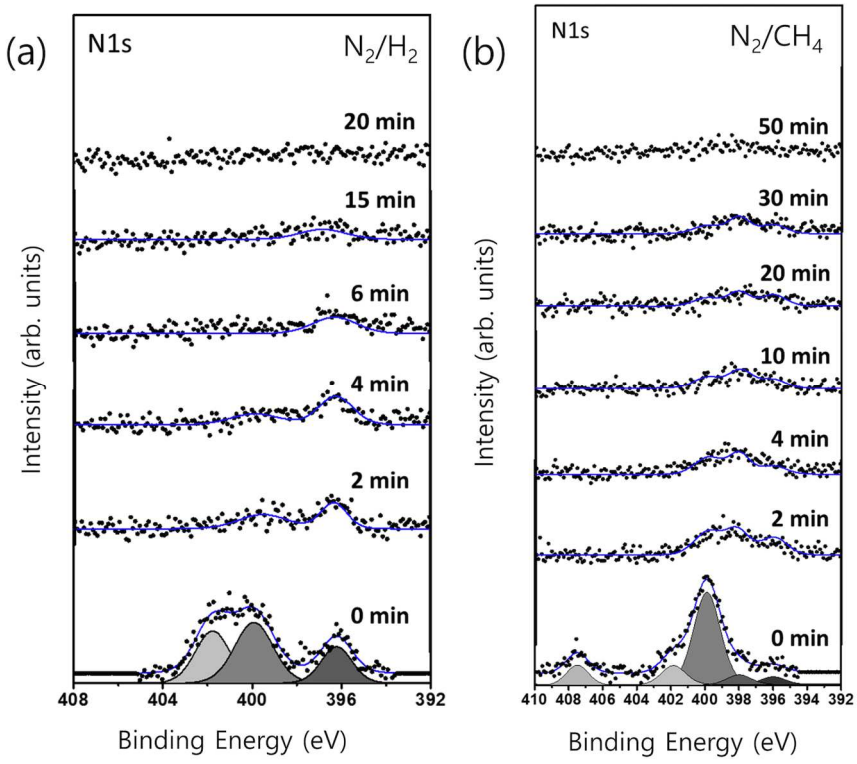


Fig. 4 XPS spectra of N 1s core level from TiO_2/Si after being exposed to the (a) N_2/H_2 and (b) N_2/CH_4 afterglows respectively at 300 °C for 30 min (Q_{tot} = 0.5slpm, P_{HF} = 100 W), which were taken after successive Ar^+ sputterings (sputter rate = 0.3 nm/min).

Since the dominant changes in the XPS spectra after the nitridation are associated with N 1s core level, those after being exposed to the N_2/H_2 and N_2/CH_4 afterglows are shown for comparison in Fig. 4. The TiO_2 film treated in the N_2/H_2 afterglow (Fig. 4a) shows similar N 1s core level features to that treated in the N_2 afterglow (Fig. S2). That is, surface N species introduced by N_2 and N_2/H_2 afterglows are characterized by two distinct N species of interstitial N (~ 400 eV) and substitutional N (~ 396 eV) species [8]. The role of H in nitridation of TiO_2 is related to surface reactions of surface N and O species with H to form volatile H_2O or NH_3 under the elevated temperature, which can affect the nitridation rate at the surface [7, 11].

For the case of N_2/CH_4, interstitial N species are more pronounced than substitutional N species. The N 1s peak at around 399 eV can be associated with the N species with direct N-C bonds. The N 1s binding energy of such N species shifts toward 400 eV with increasing number of direct N-C bonds (e.g. $N\text{-}C_3$). In addition, NO_3^- species at 407 eV is also observed [8, 25, 26]. But, it disappears right after a few min sputtering, suggesting that NO_3^- species are only present at the surface.

After the sputtering of a few nm, the films expose those N species incorporated into the sublayers of TiO_2. Here, there seems to be a distinct difference between those treated with N_2 (or N_2/H_2,) and that treated with N_2/CH_4. For the cases of N_2 and N_2/H_2 (see Fig. S2 and Fig. 4a), substitutional N species dominate with a minor contribution of interstitial N species. However, for the case of N_2/CH_4, the N 1s peak appears to be broad over 396 – 400 eV, suggesting various kinds of N species (in bonding states close to interstitial N) are introduced into the bulk [27-32]. This may be due to the effect of the co-incorporation of C atoms within the TiO_2 lattice. But, the exact concentration and bonding states of C atoms incorporated into the lattice are rather difficult to be defined since the surface C contaminant features always dominate in the C 1s spectra. Remnant C 1s feature at 284 eV after the removal of surface contaminant carbon is still quite similar to that of initial contaminant carbon in the XPS spectra (Fig. S2); only the intensity decreases. Thus, it is more likely to be that of remnant surface carbon contaminant. Even though the amount of C content is small, the trace of C 1s features at around 289 eV indicates the presence of C with direct C-O or C-N bonds (Fig. S2), which can be formed by a replacement of Ti by C [33]. No other C-related feature such as Ti-C bonding states at lower binding energies is resolved [34-36]. Even though there is no resolved C 1s feature that can be assigned to that from the reactions of C atoms in the N_2/CH_4 afterglows, we assume that the newly introduced C species are possibly present below the detection limit of XPS.

Quantification of carbon incorporation into the bulk during the treatment in the N_2/CH_4 afterglow is a difficult task since C 1s is always dominated by the contaminant carbon. Nonetheless, the quantitative analysis on the depth distribution of C atoms is also shown in Fig. S3. For all the films, C concentration decreases down to a negligible level after removing surface layers of 2 nm or so (Fig. S3), showing that most of the C content, even though not all, is due to the surface contaminant. For the case of the TiO_2 film treated in the N_2 afterglow

(Fig. S3), the C content extending down to 2 nm can be mostly assigned to those that originate from airborne contaminant. For the case of N_2/CH_4, however, the the carbon content seems to be a little bit higher than that of the N_2 only case. Despite the fact that the difference is within the measurement uncertainty, it may be due to additional carbon atoms incorporated into the bulk, even though the net amount is within the detection limit of XPS. For the case of N_2/H_2, absolute amount of the surface contaminant C is much lower than the other two cases and the sputtering readily suppress the C content below detection limit within a nm or so. A possible explanation is that reactions of TiO_2 surfaces with H atoms in the afterglow can modify the surface less vulnerable to hydrocarbon contaminant in the air when the samples are stored and handled in the ambient condition.

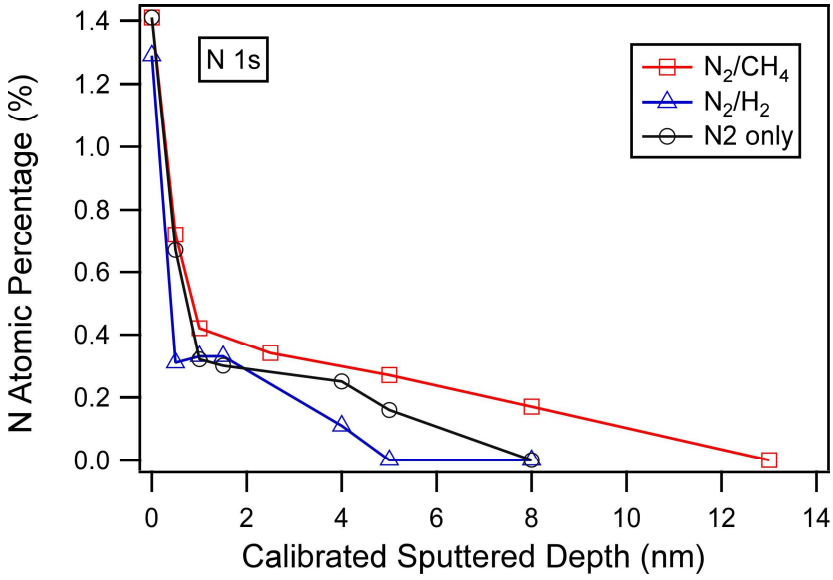


Fig. 5 Nitrogen depth profile analysis of TiO_2 films on Si after being exposed to the N_2, N_2/H_2 and N_2/CH_4 afterglows at 300 °C for 30 min (Q_{tot} = 0.5slpm, P_{HF} = 100 W) :

The quantitative analysis on the depth distribution of N species within the TiO_2 films is given in Fig. 5. It can be seen that the N species are incorporated down to about 10 nm after the treatments in the afterglows, but the exact depth varies strongly for the three cases. It increases from 5 nm for the N_2/H_2 case to 13 nm for the N_2/CH_4 case. For the N_2 only, the depth lies at 8 nm. The corresponding maximum N-atom density down to 13 nm however is quite limited to about 0.4 %, which corresponds to the [N]/[Ti] of about 1.2 %.

The incorporation of N atoms into the sublayer requires thermal activation of lattice diffusion process, which are most likely to be influenced by the substrate temperature and the process time [9, 24]. Since the treatment temperature and the time are fixed to 300 °C and 30 min for the three cases, the difference in the depth distribution must be the result of the differences in the following two processes; one is the nitriding rate at the surface under the given discharge conditions and the other is the diffusion rate of N species within the bulk. The

nitriding rate at the surface is determined by the interaction between the active species in the gas phase and the reactive sites at the surface. The substrate temperature also determines the reaction rate and the subsequent pathways of reaction products. For example, the reaction products such as H_2O and NH_3 readily desorb from the TiO_2 surface leaving vacancies at elevated temperatures [7, 37, 38]. Also, the diffusion rate of N species within the bulk can be influenced by the type of bonding states of N within the bulk as well as other impurities and crystallinity within the bulk. Thus, the difference in the depth distribution of N within TiO_2 needs to be explained not only from the surface reactions of TiO_2 with the active species in the afterglows, but also with the thermally driven processes within the bulk as well as at the surface involving all incorporated species during the treatment.

Co-doped C atoms may facilitate formation of interstitial N at the surface and subsequent diffusion into the sublayers since carbon atoms at the surface can facilitate the formation of surface oxygen vacancies at the TiO_2 surface for subsequent nitridation [39]. Especially, the co-doped carbon can facilitate the incorporation of N via the formation of C-N bonds [14, 40]. Even though no Ti-C related feature around 282 eV from C 1s core level (Fig. S2) is detected within the detection limit of XPS (which is assumed to be about 1 %), a trace of C 1s features with C-O or C-N bonds is detected (Fig. S2), which is also supported by the observation of N 1s features around 399 eV (instead of 396 eV) in Fig. 4. Incorporated carbon may replace Ti sites to make C species with direct C-O or C-N bonds. Interestingly, the formation of such C-N bonds in C,N-co-doped TiO_2 is suggested to be favored and promotes co-doping, which may lead to the extended graphitic nitride structure at high doping levels [40]. Thus, the maximum N-inclusion depth observed for the N_2/CH_4 case can be related to the high C-atoms density: [C] = 5 $10^{13}$$cm^{-3}$ with a [C]/[N] ratio of 5% as well as the reduced O-atoms impurity (one order more than O atoms).

H atoms in the N_2/H_2 afterglows was suggested to be more efficient in introducing substitutional N species at the surface [7]. The origin for the introduction of substitutional N in the N_2/H_2 case is interpreted to be the result of the chemistry of H atoms reacting with lattice oxygen atoms which leads to the removal and replacement of the O atoms by incoming N atoms to induce the formation of substitutional N. The difference in the bonding states of nitrogen at the surface can lead to such a difference in the depth distribution observed in Fig. 5.

In our previous study, diffusion into the sublayer was observed to be limited to a skin-depth layer of a few nm [7]. One of the reason is due to the fact that the sample position for the treatment in the afterglow is different between the two case studies; it is 38 cm in the quartz tube in this study, while it is in the reactor in our previous study [7]. Different densities of active species in the 18 mm quartz tube than in the reactor under the steady flowing condition are also expected to be one of the origin for such a different nitriding performance. Although the detailed origin for such a difference is believed to be an important issue for extensive future studies, it can be argued that the efficiency of nitriding in the afterglows can be controlled by choosing a proper sample position (or a tube diameter) for the treatment.

7. Conclusions

Active species densities of the N_2, N_2/H_2 and N_2/CH_4 microwave afterglows have been examined using emission spectroscopy for the use in surface nitriding of oxide materials such as TiO_2 in mind. By optimizing the flow (5 Torr, 0.5 slpm) and discharge (100 W) condition of the microwave N_2 plasma, we obtain a pink afterglow in a tube of 18 mm followed by a late afterglow.

The pink afterglow is reduced as 2% of H_2 is introduced into N_2. In the late afterglows of $N_2/<2\%H_2$ mixtures at 5 Torr and of $N_2/(0.04\text{-}0.3)\%CH_4$ mixtures at 9-13 Torr, the O-atoms from air impurity decreased strongly in density from 3.5 to 0.2 10^{13} cm^{-3} (0.5 slpm and 100 W). The flow and the discharge conditions can be optimized to maximize the active species densities such as N atoms and H (or C) atoms in the late afterglow region (z = 38 cm in the quartz tube (10^{-1}s) by monitoring the emission spectroscopy.

TiO_2 samples treated in the late afterglow for 30 min at a temperature of 300 °C are found to have a few nm thick (5 – 13 nm) oxynitride layers at the surface. However, the exact bonding nature and the thickness of the oxynitride layers are strongly determined by the type and densities of active species in the afterglow. The introduction of C atoms in the afterglows facilitates the formation of interstitial N atoms and subsequent incorporation of them into the lattice of TiO_2. The largest N-atom inclusion depth (13 nm) inside the TiO_2 target was obtained with the $N_2/0.04\%CH_4$ late afterglow in the 18 mm i.d. tube at z = 38 cm, 13 Torr, 0.5 slpm and 100 W. On the other hand, H atoms in the afterglows favor the formation and incorporation of substitutional N atoms into the bulk. Thus, our results suggest that controlled introduction of H (or C) atoms in the N atom-dominated afterglows can have a strong influence on the type of N bonding states incorporated into the oxide materials such as TiO_2 for the preparation of nanometer-thick oxynitride layers. This approach can be quite useful when oxynitride layers of a finite thickness on TiO_2 is desired as in photoelectric and photocatalytic applications.

ACKNOWLEDGMENT

This research was supported by Basic Science Research Program through the National Research Foundation of Korea (NRF) funded by the Ministry of Education, Science and Technology (NRF-2016R1D1A1B03931639, NRF-2019R1F1A1060594 and NRF-2020R1A2C1007227) and the “Human Resources Program in Energy Technology” of the Korea Institute of Energy Technology Evaluation and Planning (KETEP), granted financial resource from the Ministry of Trade, Industry & Energy, Republic of Korea. (Project No: 2017 4010 201410).

References

[1] H. Zerrouki, A. Ricard, J.P. Sarrette, Determination of N and O-atoms and N_2(A) metastable molecule densities in the afterglows of N_2-H_2, Ar-N_2-H_2 and Ar-N_2-O_2 microwave discharges, Contrib. Plasma Phys., 54 (2014) 827-837.
[2] H. Zerrouki, A. Ricard, J.P. Sarrette, Determination of N and O-atoms, of N_2(A) and N_2 (X, v>13) metastable molecules and N_2^+ ion densities in the afterglows of N_2 -H_2 , Ar-N_2 -H_2 and Ar-N_2 -O_2 microwave discharges, J. Phys. Conf. Ser., 550 (2014) 012045.
[3] M. Abdeladim, J.-P. Sarrette, A. Ricard, N.M. Maaza, Production of active species in N_2-H_2 microwave flowing discharges and afterglows: application to change of paper surface wettability, Eur. Phys. J. Appl. Phys., 67 (2014) 10801.
[4] M. Mrázková, P. Vašina, V. Kudrle, A. Tálský, C.D. Pintassilgo, V. Guerra, On the oxygen addition into nitrogen post-discharges, J. Phys. D. Appl. Phys., 42 (2009) 075202.
[5] V. Guerra, P.A. Sá, J. Loureiro, Nitrogen pink afterglow: the mystery continues, J. Phys. Conf. Ser., 63 (2007) 012007.
[6] J. Levaton, J. Amorim, A.R. Souza, D. Franco, A. Ricard, Kinetics of atoms, metastable, radiative and ionic species in the nitrogen pink afterglow, J. Phys. D. Appl. Phys., 35 (2002) 689.
[7] S. Ryu, Y. Wang, A. Ricard, J.-P. Sarrette, A. Kim, Y.K. Kim, The role of hydrogen in the nitriding of anatase TiO2 films in the N2-H2 microwave afterglows, Surf. Coat. Technol., 364 (2019) 341-346.
[8] B. Jeon, A. Kim, A. Ricard, J.-P. Sarrette, X. Yu, Y.K. Kim, A study on selective surface nitridation of TiO_2 nanocrystals in the afterglows of N_2 and N_2-O_2 microwave plasmas, Appl. Surf. Sci., 432 (2018) 163-169.
[9] X. Yu, Y. Wang, Y.K. Kim, Engineering defects and photocatalytic activity of TiO_2 nanoparticles by thermal treatments in NH3 and subsequent surface chemical etchings, Phys. Chem. Chem. Phys., 19 (2017) 24049-24058.
[10] M. D'Arienzo, N. Siedl, A. Sternig, R. Scotti, F. Morazzoni, J. Bernardi, O. Diwald, Solar Light and Dopant-Induced Recombination Effects: Photoactive Nitrogen in TiO_2 as a Case Study, J. Phys. Chem. C, 114 (2010) 18067-18072.
[11] Y. Wang, A. Ricard, J.-P. Sarrette, A. Kim, Y.K. Kim, The role of active species in the N_2 and N_2-H_2 RF afterglows on selective surface nitriding of ALD-grown TiO_2 films, Surf. Coat. Technol., 324 (2017) 243-248.
[12] A. Ricard, C. Jaoul, F. Gaboriau, N. Gherardi, S. Villeger, Production of N, H, O, and C atoms in flowing microwave discharges, Surf. Coat. Technol., 188–189 (2004) 287-293.
[13] K.V. Mironovich, D.M. Itkis, D.A. Semenenko, S.A. Dagesian, L.V. Yashina, E.Y. Kataev, Y.A. Mankelevich, N.V. Suetin, V.A. Krivchenko, Tailoring of the carbon nanowall microstructure by sharp variation of plasma radical composition, Phys. Chem. Chem. Phys., 16 (2014) 25621-25627.
[14] M. Pisarek, M. Krawczyk, M. Hołdyński, W. Lisowski, Plasma Nitriding of TiO2 Nanotubes: N-Doping in Situ Investigations Using XPS, ACS Omega, 5 (2020) 8647-8658.
[15] D. Chen, Z. Jiang, J. Geng, Q. Wang, D. Yang, Carbon and nitrogen co-doped TiO_2 with enhanced visible-light photocatalytic activity, Ind. Eng. Chem. Res., 46 (2007) 2741-2746.
[16] E. Lee, C. Park, D.W. Lee, G. Lee, H.-Y. Park, J.H. Jang, H.-J. Kim, Y.-E. Sung, Y. Tak, S.J. Yoo, Tunable Synthesis of N,C-Codoped Ti3+-Enriched Titanium Oxide Support for Highly Durable PEMFC Cathode, ACS Catal., 10 (2020) 12080-12090.
[17] X. Xu, L. Lai, J. Jiang, Z. He, S. Song, C,N-Codoped TiO2 with a Nitrogen-Doped Carbon Coating Derived from 2,6-Diaminopyridine for Visible Light-Induced Photocatalytic Hydrogen Evolution, J. Phys. Chem. C, 123 (2019) 9702-9712.
[18] A. Ricard, J.-P. Sarrette, B. Jeon, Y.K. Kim, Discharge source-dependent variation in the densities of active species in the flowing afterglows of N2 RF and UHF plasmas, Curr. Appl. Phys., 17 (2017) 945-950.
[19] B.S. Truscott, M.W. Kelly, K.J. Potter, M. Johnson, M.N.R. Ashfold, Y.A. Mankelevich, Microwave Plasma-Activated Chemical Vapor Deposition of Nitrogen-Doped Diamond. I. N2/H2 and NH3/H2 Plasmas, The Journal of Physical Chemistry A, 119 (2015) 12962-12976.
[20] A. Ricard, H. Malvos, S. Bordeleau, J. Hubert, Production of active species in a common flowing post-discharge of an Ar-N2plasma and an Ar-H2-CH4plasma, J. Phys. D. Appl. Phys., 27 (1994) 504-508.

[21] G.M. Provencher, D.J. McKenney, CN Emission in Active Nitrogen. II. The Role of Energy Transfer and Atom Transfer Reactions in CN(X2Σ+) Excitation, Canadian Journal of Chemistry, 50 (1972) 2527-2536.
[22] K.V. Mironovich, Y.A. Mankelevich, D.G. Voloshin, S.A. Dagesyan, V.A. Krivchenko, Simulation and optical spectroscopy of a DC discharge in a CH4/H2/N2 mixture during deposition of nanostructured carbon films, Plasma Physics Reports, 43 (2017) 844-857.
[23] F. Leonori, D. Skouteris, R. Petrucci, P. Casavecchia, M. Rosi, N. Balucani, Combined crossed beam and theoretical studies of the C(1D) + CH4 reaction, The Journal of Chemical Physics, 138 (2013) 024311.
[24] Y.K. Kim, S. Park, K.-J. Kim, B. Kim, Photoemission study of N-doped TiO_2(110) with NH_3, J. Phys. Chem. C, 115 (2011) 18618-18624.
[25] J. Baltrusaitis, P.M. Jayaweera, V.H. Grassian, XPS study of nitrogen dioxide adsorption on metal oxide particle surfaces under different environmental conditions, Phys. Chem. Chem. Phys., 11 (2009) 8295-8305.
[26] J.A. Rodriguez, T. Jirsak, G. Liu, J. Hrbek, J. Dvorak, A. Maiti, Chemistry of NO_2 on oxide surfaces: Formation of NO_3 on TiO_2(110) and NO_2↔O vacancy interactions, J. Am. Chem. Soc., 123 (2001) 9597-9605.
[27] M. Sathish, B. Viswanathan, R.P. Viswanath, C.S. Gopinath, Synthesis, characterization, electronic structure, and photocatalytic activity of nitrogen-doped TiO_2 nanocatalyst, Chem. Mater., 17 (2005) 6349-6353.
[28] X. Chen, C. Burda, Photoelectron spectroscopic investigation of nitrogen-doped titania nanoparticles, J. Phys. Chem. B, 108 (2004) 15446-15449.
[29] F. Peng, L. Cai, L. Huang, H. Yu, H. Wang, Preparation of nitrogen-doped titanium dioxide with visible-light photocatalytic activity using a facile hydrothermal method, J. Phys. Chem. Solids, 69 (2008) 1657-1664.
[30] P. Romero- Gómez, V. Rico, A. Borrás, A. Barranco, J.P. Espinós, J. Cotrino, A.R. González-Elipe, Chemical state of nitrogen and visible surface and Schottky barrier driven photoactivities of N-doped TiO_2 thin films, J. Phys. Chem. C, 113 (2009) 13341-13351.
[31] C. Chen, H. Bai, C. Chang, Effect of plasma processing gas composition on the nitrogen-doping status and visible light photocatalysis of TiO_2, J. Phys. Chem. C, 111 (2007) 15228-15235.
[32] P.G. Smirniotis, T. Boningari, D. Damma, S.N.R. Inturi, Single-step rapid aerosol synthesis of N-doped TiO2 for enhanced visible light photocatalytic activity, Catalysis Communications, 113 (2018) 1-5.
[33] I. Ruzybayev, S.S. Baik, A.K. Rumaiz, G.E. Sterbinsky, J.C. Woicik, H.J. Choi, S. Ismat Shah, Electronic structure of C and N co-doped TiO2: A combined hard x-ray photoemission spectroscopy and density functional theory study, Appl. Phys. Lett., 105 (2014) 221605.
[34] W. Mai, F. Wen, D. Xie, Y. Leng, Z. Mu, Structure and composition study of carbon-doped titanium oxide film combined with first principles, Journal of Advanced Ceramics, 3 (2014) 49-55.
[35] C.X. Dong, Y.J. Wang, XPS investigation of carbon-doped TiO2 photocatalysts, in: World Automation Congress 2012, 2012, pp. 1-4.
[36] G. Liu, C. Han, M. Pelaez, D. Zhu, S. Liao, V. Likodimos, N. Ioannidis, A.G. Kontos, P. Falaras, P.S.M. Dunlop, J.A. Byrne, D.D. Dionysiou, Synthesis, characterization and photocatalytic evaluation of visible light activated C-doped TiO2nanoparticles, Nanotechnol., 23 (2012) 294003.
[37] B. Kim, B.D. Kay, Z. Dohnálek, Y.K. Kim, Ammonia Formation from NO Reaction with Surface Hydroxyls on Rutile TiO2(110)-1 × 1, J. Phys. Chem. C, 119 (2015) 1130-1135.
[38] Z. Dohnálek, I. Lyubinetsky, R. Rousseau, Thermally-driven processes on rutile TiO_2(110)-(1×1): A direct view at the atomic scale, Progress in Surface Science, 85 (2010) 161-205.
[39] J. Graciani, Y. Ortega, J. Fdez. Sanz, Carbon Doping of the TiO2 (110) Rutile Surface. A Theoretical Study Based on DFT, Chem. Mater., 21 (2009) 1431-1438.
[40] A.V. Raghu, K.K. Karuppanan, B. Pullithadathil, Controlled Carbon Doping in Anatase TiO2 (101) Facets: Superior Trace-Level Ethanol Gas Sensor Performance and Adsorption Kinetics, Advanced Materials Interfaces, 6 (2019) 1801714.

Graphical Abstract

